

7 *Active Surface Wave Attenuation Estimation*

“Think as I think,” said a man,
“Or you are abominably wicked;
You are a toad.”

And after I had thought of it,
I said: “I will, then, be a toad.”

Stephen Crane

7.1 Introduction

The ability to estimate correct attenuation coefficients impacts the ability to reliably invert a damping ratio profile. This statement has meaning at two levels. First, attenuation estimates at individual frequencies affect the inverted damping ratio profile at depths proportional to that frequency-specific wavelength. Second, just as in phase velocity, attenuation coefficients stem from a convolution of the material damping ratios from the surface to a depth proportional to the wavelength, weighted by an eigenfunction, and therefore, attenuation estimates at a specific depth depend on the material damping properties from the surface to that depth. Consequently, misestimating the attenuation coefficient over a relatively small range of frequencies or wavelengths, for example 10 to 20 m, will impact the damping ratio profile estimate over a larger range of depth, since the attenuation coefficient at depths greater than 20 m include contributions from the material properties at depths of 10 to 20 m.

Similar to phase velocity estimation, traditional material attenuation estimators suffer several major limitations. Several of the major problems commonly associated with the experimental determination of attenuation are discussed. This chapter then discusses the physics of wave attenuation. The same general equation governs energy attenuation in both cylindrical and plane wavefields, and the introduction of the general wave attenuation model will allow an easier transition to the passive attenuation estimation methods introduced in Chapter 8. Next, the optimum sub-array cylindrical, dominant mode attenuation estimator

is introduced and applied to the ISC '98 experimental data. Building on the dominant mode attenuation derivation, multiple mode sub-array attenuation coefficients are then estimated for the ISC '98 site.

7.2 The Categories of Traditional Attenuation Estimation Limitations

Traditional geotechnical attenuation estimates have suffered from three major limitations:

- 1.) Incorrect physical and geometric spreading model,
- 2.) Inability to remove noise optimally,
- 3.) Inability to introduce and account for multiple modes.

The model incompatibility represents the greatest impediment to improving attenuation estimates and has produced an unnecessarily complicated attenuation model. The inability to remove noise optimally introduces varying noise power into the attenuation estimate, and the inability to account for multiple modes leads to incorrect attenuation estimates.

7.3 The Physics of Seismic Wave Attenuation

The same general equation governs wave propagation in cylindrical and plane wavefields, which means the two motions can be modeled by identical parameters. The parameters include the amplitude, wavenumbers, and a complex-scaling model. The cylindrical and plane wave attenuation estimators must be considered separately due to a difference in the experimentally relevant parameters in each case. The general equation will be introduced, and then the relevant parameters for the cylindrical wave model will be discussed. Chapter 8 discusses the relevant plane wave parameters.

7.3.1 General Wave Motion Model

A single surface wave propagating with a single frequency and single wavelength in a dissipative medium can be described with the following equation:

$$u(\mathbf{k}, \mathbf{x}, \omega, t) = A_0(\mathbf{k}, \omega) e^{-\alpha(\mathbf{k}, \omega) \mathbf{x}} e^{j\omega t} R(\mathbf{k}, \mathbf{x}) \quad (7.1)$$

where $u(\mathbf{k}, \mathbf{x}, \omega, t)$ = the measured displacement at spectral components \mathbf{k} and ω and at vector position \mathbf{x} and time t , A_0 = initial amplitude of the propagating wave, α = the material attenuation coefficient, $e^{j\omega t}$ = harmonic time dependence, and $R(\mathbf{k}, \mathbf{x})$ = a complex-valued scaling function, which includes phase and geometric spreading information.

The important features of the model include the following:

- 1.) Material attenuation α - The attenuation of wave energy in a vertically heterogeneous soil profile is a material parameter that is a function only of frequency and wavenumber,
- 2.) Governing geometric model R (R for Rayleigh) - Depending on the geometry of the problem, i.e. either plane wave or cylindrical, R equals a complex exponential or Hankel function solution to the plane or cylindrical wave equation, respectively, evaluated at the argument (\mathbf{k}, \mathbf{x}) ,

- 3.) Amplitude A_0 - The wave amplitude at some reference position x_0 and reference time t_0 .

If multiple waves are present in the wavefield, superposition sums yield the model of the motion. The dependence of the geometric model R and material attenuation on frequency and wavenumber displays an intimate relationship with the dispersion relation. To allow clear insight into the nature of the material attenuation estimates, especially for the dominant mode, the derivations will consider only single signal wavefields.

7.3.2 Overview of Material Attenuation with General Model

Using the general model and two reference points along a linear axis, consider a single wave propagating with a single amplitude A_0 at a single frequency ω_0 , single wavenumber k_0 , and single attenuation coefficient α_0 . Since the motion is at a single temporal frequency, and using a fixed reference time, the dependency on the temporal motion characteristics can be suppressed, allowing focused attention on the spatial properties of the model. If material attenuation equals zero, the displacements u measured at the two positions x_1 and x_2 along the linear axis, where x_1 is closer to the signal source, equal

$$\begin{aligned} u(k_0, x_1) &= A_0(k_0)R(k_0, x_1) \\ u(k_0, x_2) &= A_0(k_0)R(k_0, x_2) \end{aligned} \quad (7.2)$$

where the motion u is complex-valued, the real-valued part corresponding to the actual motion, and the function R yields a complex-valued scaling of the amplitude A_0 , i.e. a change in the magnitude and phase of the motion. The complex-valued scaling factor between the two positions x_1 and x_2 is given by

$$\frac{u(k_0, x_2)}{u(k_0, x_1)} = \frac{A_0(k_0)R(k_0, x_2)}{A_0(k_0)R(k_0, x_1)} = \frac{R(k_0, x_2)}{R(k_0, x_1)} \quad (7.3)$$

For a plane wave, the amplitude A_0 would not decay, but the phase of the motion would change as the wave propagated from point 1 to 2. For a cylindrical wave, the function R determines the phase change and the geometric spreading of the energy, and therefore, the amplitude A_0 would decrease as the wave propagates from position 1 to 2. If the positions x_1 and x_2 happen to be in the far-field of a cylindrical wavefield, the decay rate will tend to $\sqrt{\Delta x}$, where Δx = the change in distance from position 1 to 2.

Introducing material attenuation into the model, the displacements at x_1 and x_2 equal

$$\begin{aligned} u(k_0, x_1) &= A_0(k_0)e^{-\alpha(k_0)x_1}R(k_0, x_1) \\ u(k_0, x_2) &= A_0(k_0)e^{-\alpha(k_0)x_2}R(k_0, x_2) \end{aligned} \quad (7.4)$$

The complex-valued scaling of motion between position x_1 and x_2 now equals

$$\frac{u(k_0, x_2)}{u(k_0, x_1)} = \frac{A_0(k_0)e^{-\alpha(k_0)x_2} R(k_0, x_2)}{A_0(k_0)e^{-\alpha(k_0)x_1} R(k_0, x_1)} = e^{-[\alpha(k_0)(x_2 - x_1)]} \frac{R(k_0, x_2)}{R(k_0, x_1)} \quad (7.5)$$

Notice the original wave amplitude A_0 always cancels out, indicating the relative nature of material attenuation. Considering Equation 7.5 as a filter or linear system places the attenuation problem into a more common perspective. The output $u(x_2)$ equals the input $u(x_1)$ scaled by a complex-valued filter coefficient defined entirely by the wavenumber and attenuation coefficient, and therefore, the following equation represents the site transfer function

$$\frac{u(x_2)}{u(x_1)} = e^{-\alpha(x_2 - x_1)} \frac{R(k_0, x_2)}{R(k_0, x_1)} \quad (7.6)$$

The function $\frac{R(k_0, x_2)}{R(k_0, x_1)}$ equals the phase change and geometric spreading due to the site-specific wavenumbers, and therefore, is a function of the same parameters as the dispersion curve, i.e. wavenumber and frequency. In plane wave analysis, geometric spreading will not be a factor, yielding a $\left| \frac{R(k_0, x_2)}{R(k_0, x_1)} \right| = 1$ for all frequencies and wavenumbers. The difference in the functions $R(\mathbf{k}, \mathbf{x})$ represents the *only* physical model difference in material attenuation estimation for the plane and cylindrical wave cases.

7.3.3 Cylindrical Wave Motion Model

Cylindrical wave motion emanating from an active point source follows the following model:

$$u(k_x, x, \omega, t) = Ae^{-\alpha(k_x, \omega)x} H_0(k_x, x) \quad (7.7)$$

where, since the disturbance is symmetric around the source, the motion is parameterized by the scalar wavenumber k_x . The function $R(\mathbf{k}, \mathbf{x})$ equals a Hankel function in this case. In all the analyses included in the following sections, time is removed as a factor because the wave motion is viewed at a fixed time.

The important properties of this model, *vis a vis* the passive plane wave problem, include the following:

- 1.) The geometric spreading of cylindrical waves is parameterized solely by the site characteristic wavenumbers k_x at frequencies ω . Therefore, the wavenumber contains information about velocity, direction, and geometric energy spreading,
- 2.) The zeros of the displacement function across space are unequally spaced.

The complex-valued scaling of the amplitude between any two points on a linear axis from the source becomes, suppressing temporal frequency and temporal dependence,

$$\frac{u(k_x, x_2)}{u(k_x, x_1)} = \frac{A_0 e^{-\alpha(k_x) x_2} H_0(k_x, x_2)}{A_0 e^{-\alpha(k_x) x_1} H_0(k_x, x_1)} = e^{-[\alpha(k_x)(x_2 - x_1)]} \frac{H_0(k_x, x_2)}{H_0(k_x, x_1)} \quad (7.8)$$

The use of the model in Equation 7.8 will allow optimum estimates of the dominant mode attenuation and extraction of multimode attenuation coefficients.

7.4 Noise Removal or Minimization

In traditional attenuation estimates, the background seismic noise has not adequately been considered. The typical noise removal techniques do not minimize noise power in any optimizing fashion, and in nonstationary noise environments, the noise removal techniques increase uncertainty in the estimates. This section discusses the effects of noise inclusion and possible noise removal alternatives.

7.4.1 Stationary Noise Inclusion Leads to Conservative Attenuation Estimates

If the background seismic noise field exhibits stationary statistics at each frequency of interest, inclusion of the noise in the estimation process leads to conservative (i.e. too low) material attenuation estimates. Consider a simple plane wavefield example, consisting of a single wave with amplitude = 10 at position $x_1 = 0$ m, and amplitude = 8 at position $x_2 = 10$ m. Assume a stationary background noise field is also present in the measurements, where the noise measured at the two locations is independent, identically distributed white Gaussian noise, and the spectral amplitude of the noise = 3 at the frequency of interest. Viewing attenuation as the relative decline of energy between two points, referenced by the original amplitude, the attenuation coefficients for the *include noise* and *remove noise* cases are the following:

Include Stationary Noise:

$$\frac{A_1(\text{Signal} + \text{Noise}) - A_2(\text{Signal} + \text{Noise})}{A_1(\text{Signal} + \text{Noise})} = \frac{(10 + 3) - (8 + 3)}{10 + 3} = \frac{2}{13} = 0.15$$

$$\text{Attenuation}_{(\text{Signal} + \text{Noise})} = \frac{0.15}{10\text{m}} = 0.015 \text{ (1/m)}$$

Remove Stationary Noise:

$$\frac{A_1(\text{Signal}) - A_2(\text{Signal})}{A_1(\text{Signal})} = \frac{(10) - (8)}{10} = \frac{2}{10} = 0.20$$

$$\text{Attenuation}_{(\text{Signal})} = \frac{0.2}{10\text{m}} = 0.020 \text{ (1/m)}$$

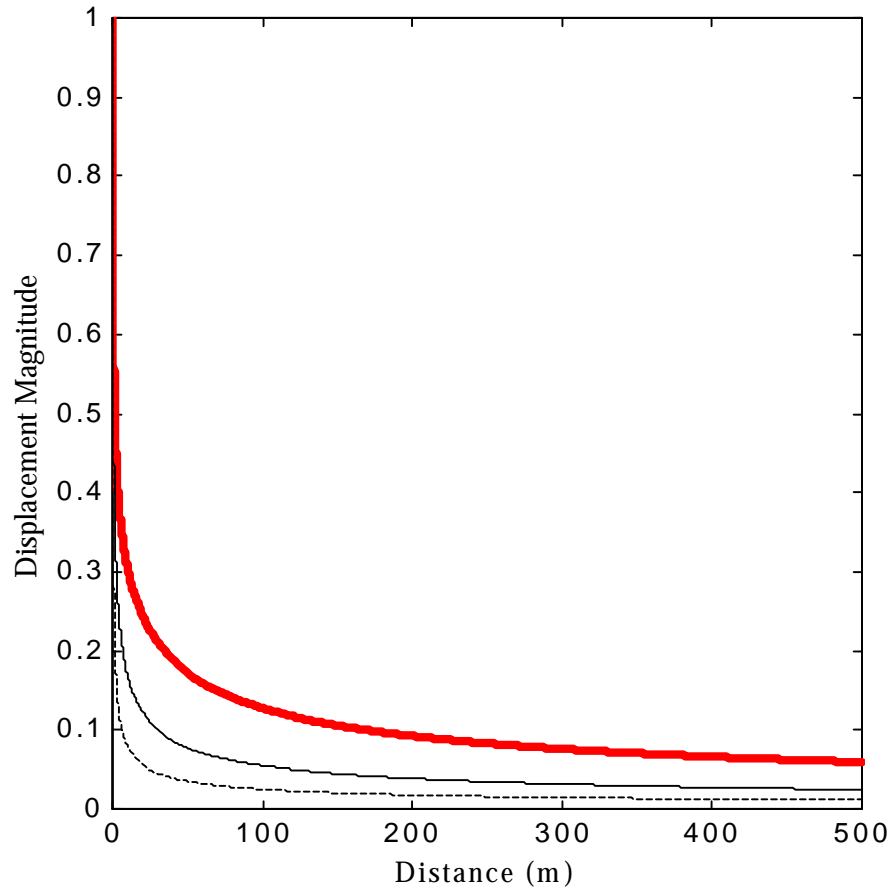


Figure 7.1 Energy Decay in Cylindrical Wavefield for Various Wavenumbers. The geometric energy decay in a cylindrical wavefield, i.e. for a Bessel function solution, is shown for wavenumber = 0.01 rad/m (thick line), 0.1 rad/m (solid line), and 1 rad/m (dashed line).

In this case, a higher attenuation estimate results from removing noise. The nonstationary noise power case introduces the possibility of increasing energy as a function of distance. The simple example frames the discussion regarding the effects of trying to correct noisy measurements. The traditional methods of noise correction increase the estimate uncertainty under certain circumstances, which has undesirable consequences on the inverted damping ratio soil profile.

7.4.2 Advanced Noise Removal Methods

Advanced noise removal, estimation, and cancellation techniques exist in advanced digital signal processing. Adaptive noise cancellation in nonstationary environments represents the optimum solution, especially in active seismic surface wave testing due to

complete control over the source characteristics. Noise reduction for active surface wave measurements must consider the two following problems:

- 1.) Competing signals,
- 2.) Ambient, background seismic noise.

Reduction of the effects of competing signals depends on sub-array analyses, and the effects of the competing signals are reduced to the extent that the sub-array spatial filter has good sidelobe and mainlobe characteristics. Reduction of ambient, background seismic noise present in all sensor measurements represents a separate problem. The reduction of both types of effects are discussed in Section 7.6.

7.5 Material Attenuation in a Cylindrical Wavefield

Geometric spreading of energy is controlled by all the wavenumbers present in the wavefield. The \sqrt{x} decay rate is only an approximation. Once geometric spreading is

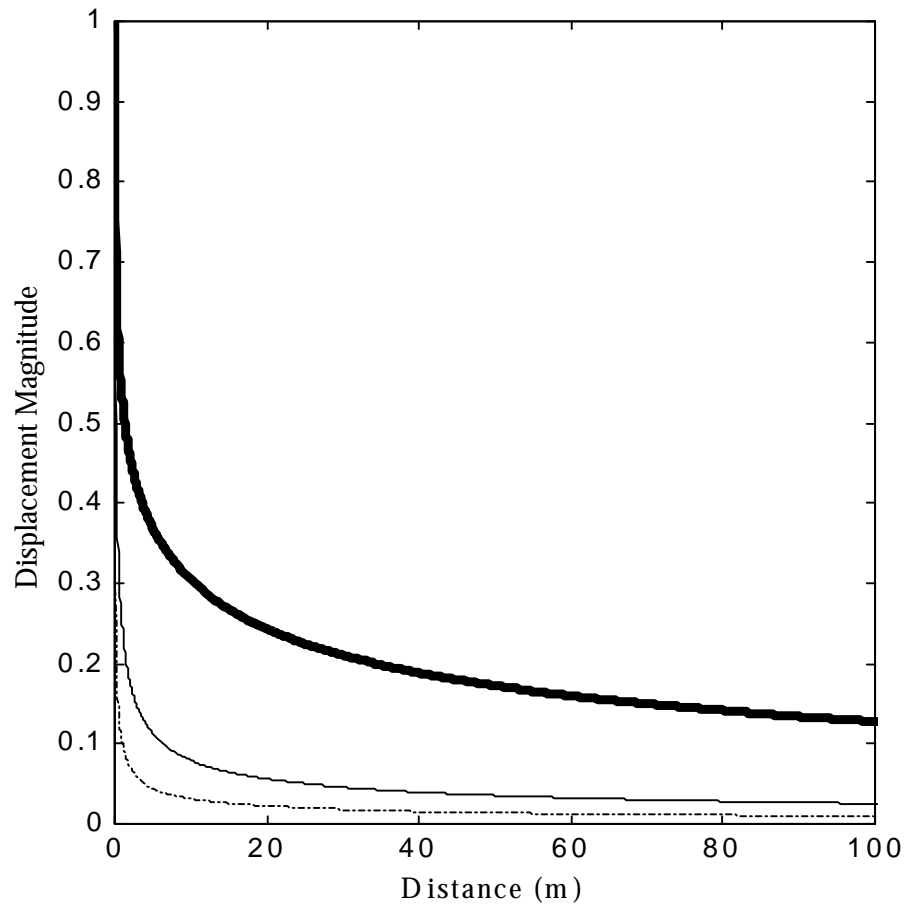


Figure 7.2 Cylindrical Wavefield Solution Versus the Far-Field, \sqrt{x} Model. The cylindrical, Bessel function solution for wavenumbers = 0.01 rad/m (dark, thick line) and 1 rad/m (solid line), and the far-field, \sqrt{x} decay solution (dashed-dot line) are shown.

removed, shorter wavelength modes control amplitude oscillations around the longest wavelength mode. This section will discuss the cylindrical wavefield model and Section 7.7 will discuss the effects of the model incompatibility.

7.5.1 Geometric Spreading

Geometric spreading of cylindrically propagating Rayleigh surface waves is completely determined by the wavenumbers present in the wavefield. Different wavenumbers decay at different rates, explaining the previously perceived deviation from the \sqrt{x} decay rate (Lai, 1998). Figure 7.1 shows the decay of energy of a cylindrical wavefield, parameterized by various wavenumbers with equal amplitudes, in a medium with no material attenuation. Lower wavenumbers decay less rapidly than larger wavenumbers,

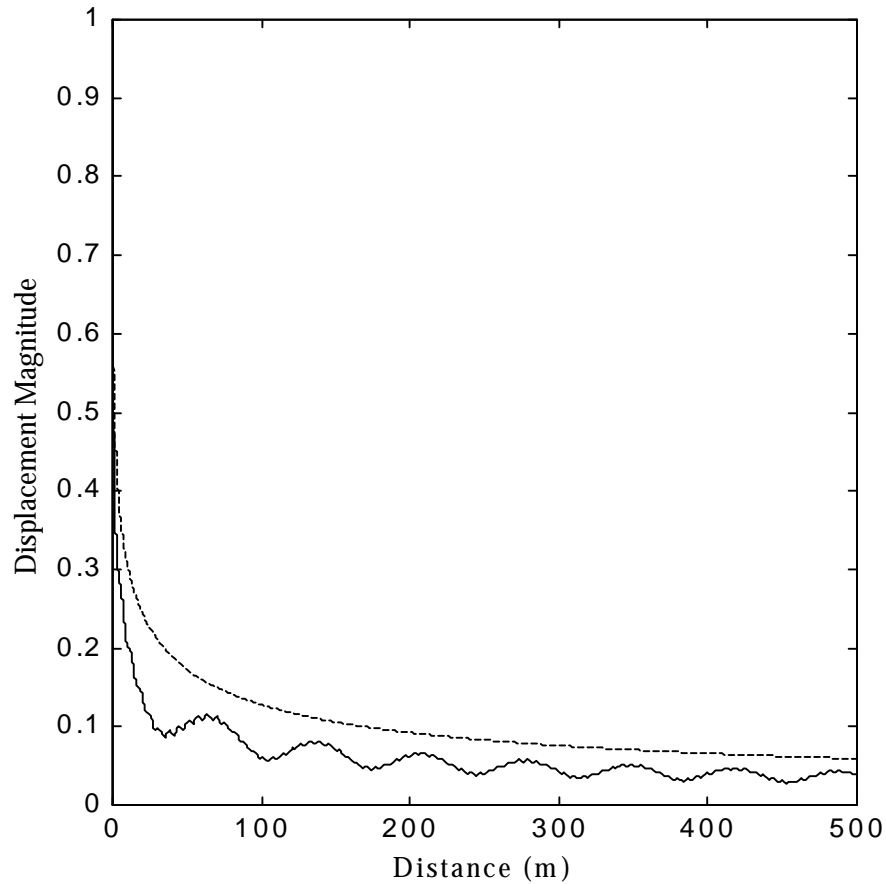


Figure 7.3 Multiple Mode Cylindrical Wavefield Superposition. The multiple mode normalized motion for a cylindrical wavefield containing wavenumbers equal to 0.01, 0.1 and 1 rad/m, with amplitudes equal to 3, 2 and 1, respectively, is shown with the solid line. The dominant mode wavefield decay is shown for reference with the dashed line. Notice that the decay rate of the dominant mode and the superposed wavefield differ.

all wavenumbers tend to a \sqrt{x} as the distance from the origin increases, and the larger wavenumbers tend to the \sqrt{x} decay rate more quickly than smaller wavenumbers.

To place the far-field, \sqrt{x} decay rate in perspective, Figure 7.2 shows the cylindrical solution for two wavenumbers and the \sqrt{x} solution for equal amplitude waves. The \sqrt{x} decays more rapidly than the cylindrical wavefields near the source, and for the distance shown in the figure, neither cylindrical wavefield has reached the \sqrt{x} decay rate. Section 7.7 will compare the cylindrical and far-field, \sqrt{x} solutions more completely.

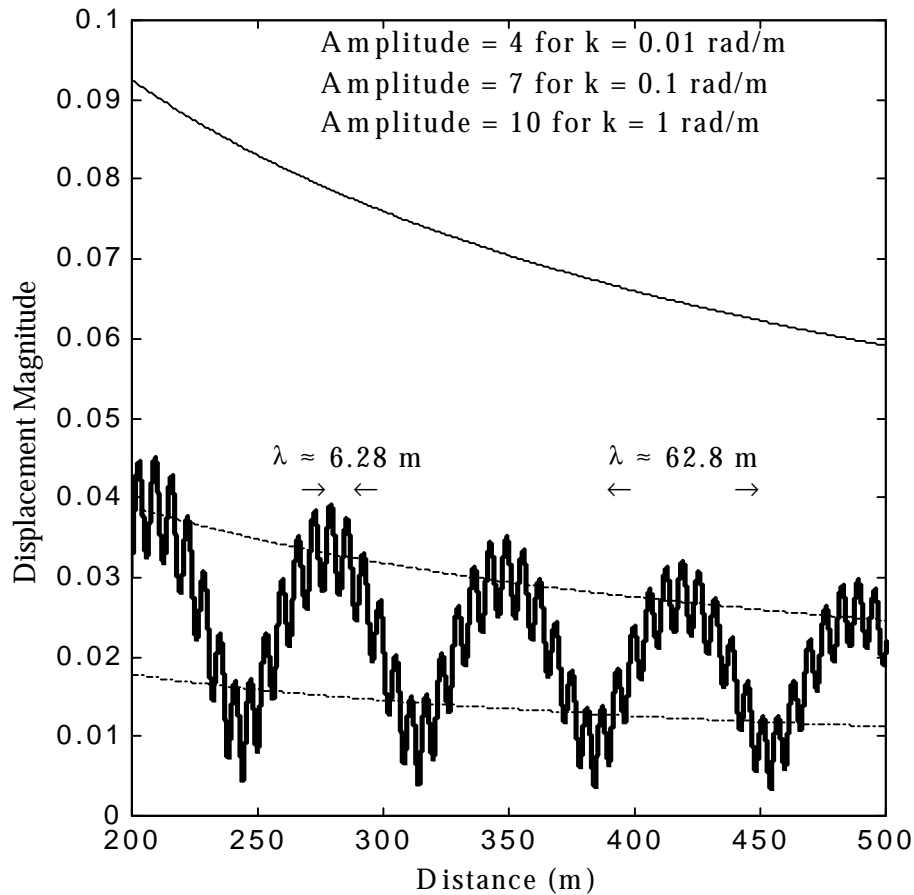


Figure 7.4 Superposition of Multiple Cylindrical Modes. The motion for a cylindrically spreading wavefield containing three modes (thick, solid line) with wavenumbers and amplitudes in the upper right corner is shown. The wavefield for single cylindrical wavenumbers equal to 0.01 rad/m (solid line), 0.1 rad/m (dashed line), and 1 rad/m (dashed-dot line) are shown for reference. Notice that the wavelengths corresponding to the larger wavenumbers control the oscillation around the lowest wavenumber.

7.5.2 Modal Magnitude Superposition

Superposition of Bessel functions displays several important qualities. First, although dominated by the dominant wavenumber, geometric spreading of energy is a function of all modal wavenumbers present in the wavefield. Second, in magnitude measurements, shorter wavelengths control the oscillation of the measurements around the longest wavelength mode. This section will discuss these two major qualities in detail, offering figures to aid in the visualization of cylindrical wavefields.

Figure 7.3 shows a multiple mode, cylindrical wavefield, with the dominant mode wavenumber shown for reference. The superposed motion shows a different decay rate than the dominant mode. Additionally, the superposed motion shows an oscillatory character. Figure 7.4 shows a closer view of the oscillation of a multimodal, cylindrical wavefield. The oscillations around the longest wavelength mode are controlled by the shorter wavelength modes. The difference in the decay rates for site-specific layered soil profiles is explained by the difference in the site-specific wavenumbers.

Figure 7.5 shows the progression of cylindrical wavefield displacement magnitudes as the dominant mode changes from wavenumber = 0.01 rad/m to wavenumber = 0.1 rad/m. Figure 7.5 (a.) shows the displacements in a wavefield dominated by a wavenumber equal to 0.01 rad/m. The decay of the motion completely follows the dominant wavenumber. As the relative amplitude of the second wavenumber = 0.1 rad/m increases, the motions begin to oscillate, but the dominant wavenumber still tends to control the decay of energy, as shown in Figure 7.5 (b.). Figures 7.5 (c. to f.) show the progressive change in the wavefield as the dominant wavenumber changes from 0.01 rad/m to 0.1 rad/m. When the

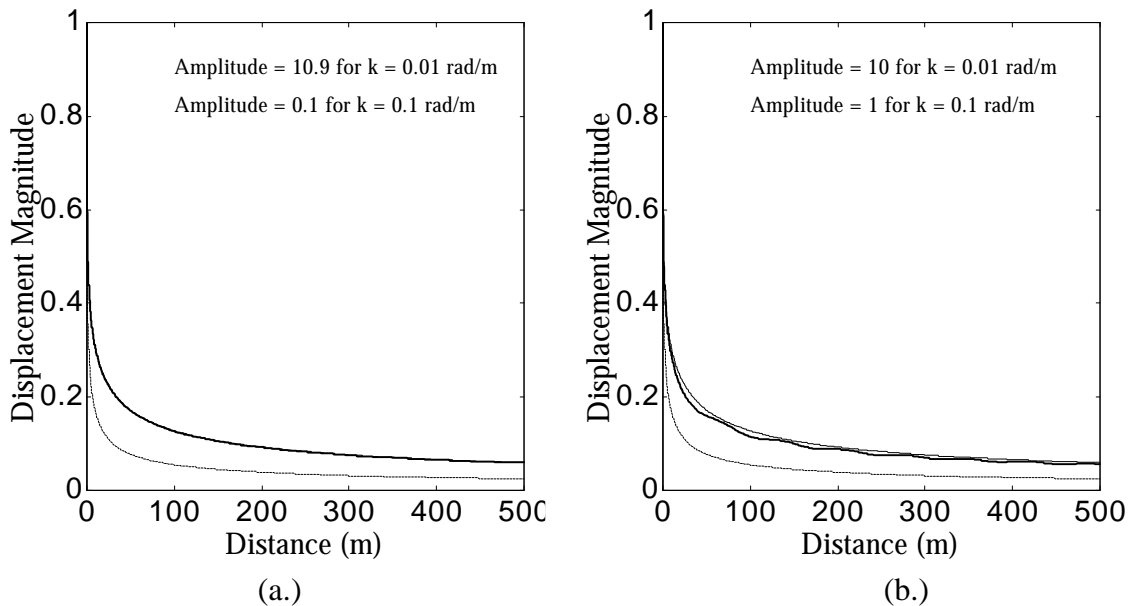


Figure 7.5 (a. and b.) Progression of Cylindrical Wavefield Displacement as Dominant Mode Changes from Wavenumber = 0.01 rad/m to Wavenumber = 0.1 rad/m. In all figures, the decay for wavenumbers equal to 0.01 rad/m (light, solid line), 0.1 rad/m (dashed line), and the superposed wavefield (dark, solid line) are shown.

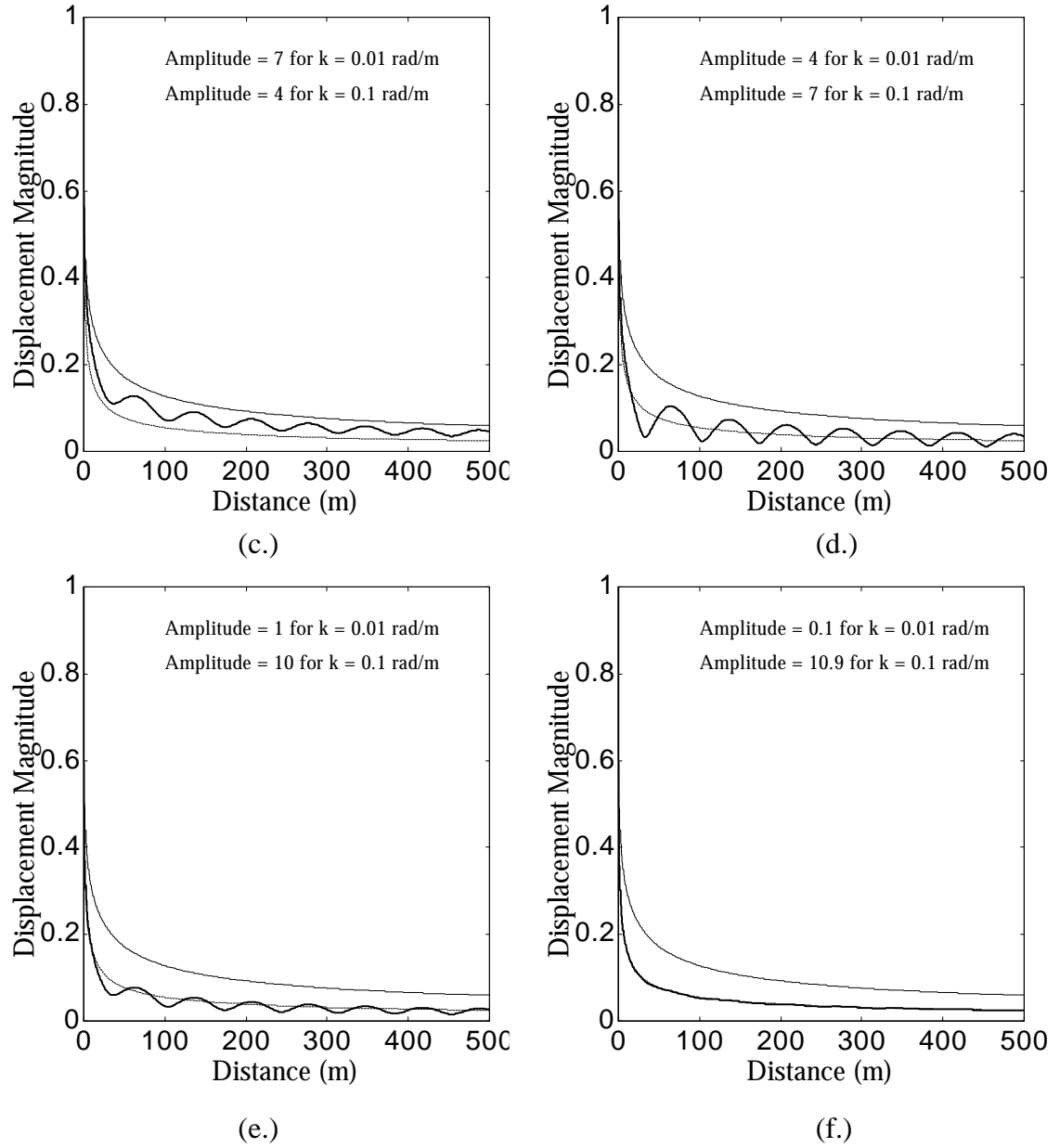


Figure 7.5 (c. to f.) Progression of Cylindrical Wavefield Displacement as Dominant Mode Changes from Wavenumber = 0.01 rad/m to Wavenumber = 0.1 rad/m. In all figures, the decay for wavenumbers equal to 0.01 rad/m (light, solid line), 0.1 rad/m (dashed line), and the superposed wavefield (dark, solid line) are shown.

wavenumber 0.1 rad/m dominates, the energy decreases at a greater rate than when a wavenumber of 0.01 rad/m dominates.

7.6 Attenuation Coefficient Estimation

To obtain optimum attenuation coefficient estimates, geometric spreading must be removed with the correct physical model. Removing geometric spreading becomes a

normalization using the combined effects of the wavenumbers estimated in Chapter 6. After removing geometric spreading, a limiting attenuation coefficient, corresponding to the smallest wavenumber as function of frequency, can be estimated. Modal attenuation coefficients for the modes containing the dominant and second greatest energy are also estimated using sub-arrays. The attenuation coefficients are estimated for the ISC '98 site.

7.6.1 Geometric Spreading Removal

After determining the dispersion relation, the experimentally measured complex-valued displacements can be normalized to remove geometric spreading effects. If $u(\omega, x)$ are the complex-valued experimental measurements, the normalized displacements equal

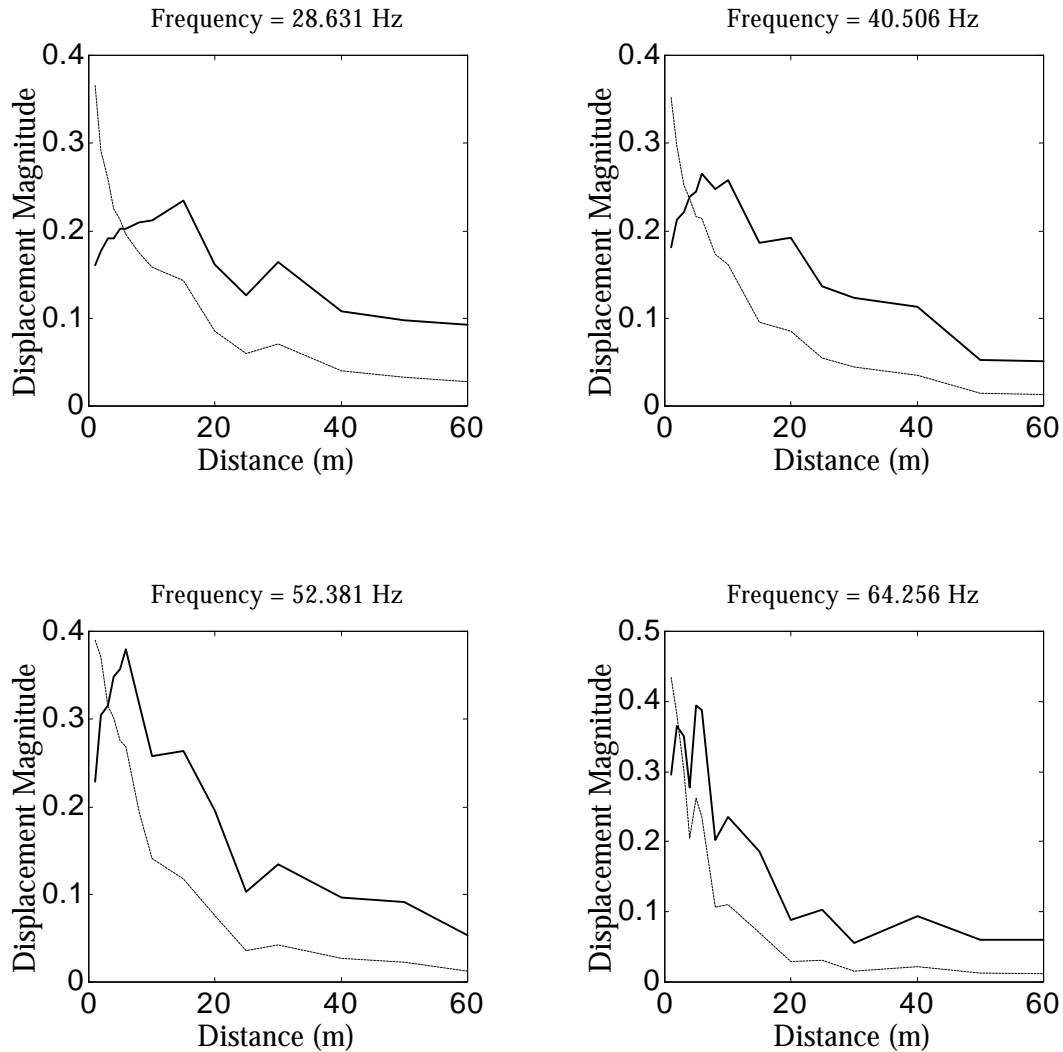


Figure 7.6 Experimental Measurements from ISC '98 Site Normalized for Cylindrical Wavenumber Geometric Spreading. The displacement magnitudes (dashed lines) for several frequencies have been normalized by the geometric spreading due to the two wavenumbers containing the greatest energy (solid lines).

$$u_{\text{normalized}}(\omega, x) = \frac{u(\omega, x)}{\sum_m A_m(\mathbf{k})R(\mathbf{k}, x)} \quad (7.9)$$

where $\sum_m A_m(\mathbf{k})R(\mathbf{k}, x)$ equals the summation of the function $R(\mathbf{k}, x)$, weighted by the modal amplitudes A_m , over the m cylindrical modes present in the wavefield at the frequency ω . The modal functions $R(\mathbf{k}, x)$ and their amplitude ratios are determined experimentally and used to normalize the experimental measurements.

Figure 7.6 shows the displacement magnitudes for the experimental measurements and with geometric spreading removed. Geometric spreading was removed by using the

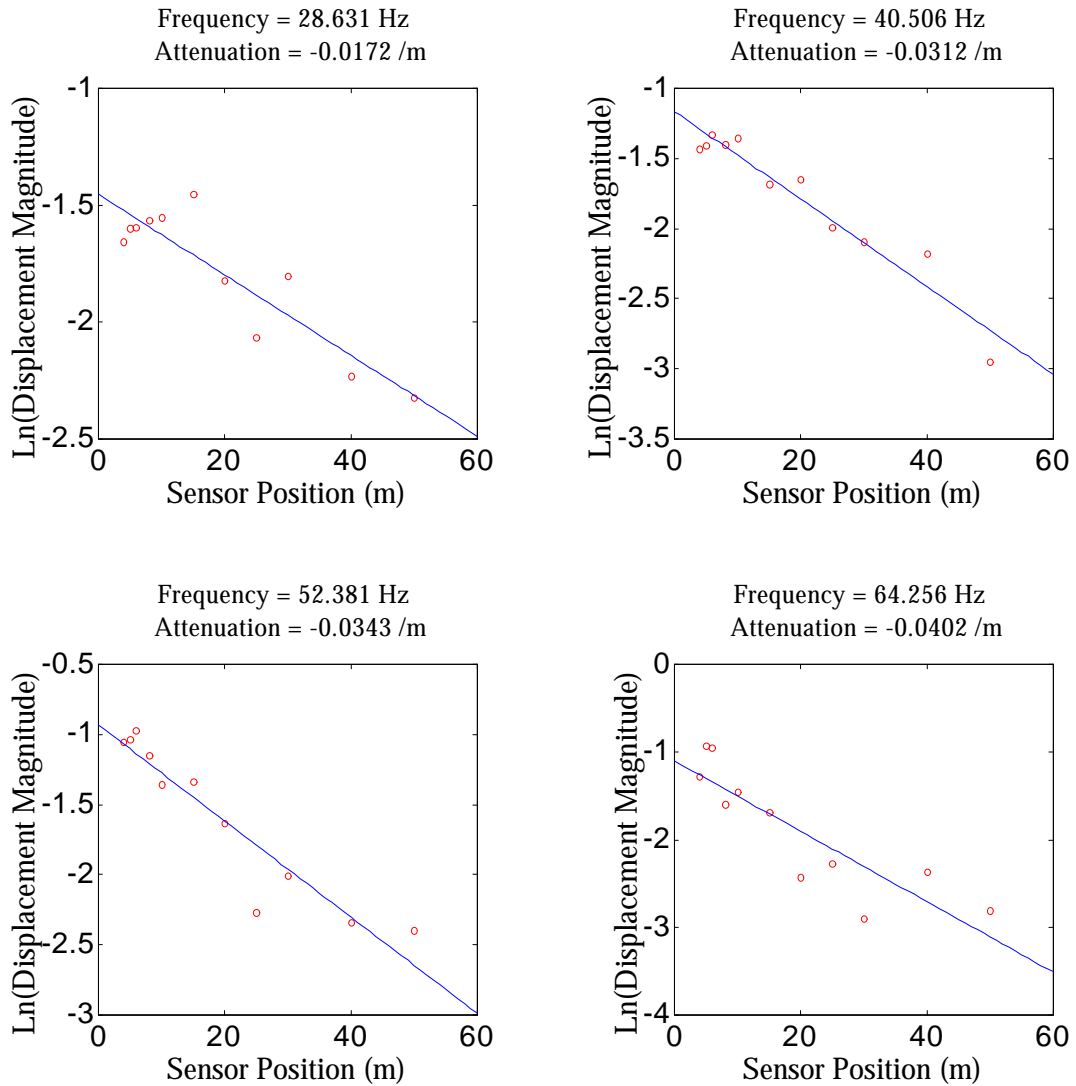


Figure 7.7 ISC '98 Attenuation Coefficient Estimates from Least Squares Fitting the Geometric Spreading Normalized Displacements

two wavenumbers containing the greatest energy and their amplitude ratios, as estimated in Chapter 6. Two notable features of the corrected displacements are the following:

- 1.) The normalized displacement magnitudes increase near the source due to the creation of multiple surface wave modes,
- 2.) The corrected displacements become more linear, similar to plane wave motion, due to the removal of the cylindrical spreading effects.

7.6.2 Minimum Wavenumber Attenuation Coefficient Estimation

Recall that the superposition of modes yields a magnitude measurement with the shorter wavelengths (larger wavenumbers) oscillating around the longest wavelength (shortest wavenumber). If the measurements cover a large enough spatial distance to allow complete orthogonality of the multiple modes, least squares fitting a line to all the normalized displacements yields an attenuation coefficient that corresponds to the minimum wavenumber. Figure 7.7 shows the attenuation coefficient estimated at four frequencies. Almost sinusoidal oscillation around the main trend is evident.

The attenuation curve from this estimation technique is shown in Figure 7.8. The waviness at the lower frequencies is probably due to varying amounts of orthogonality and

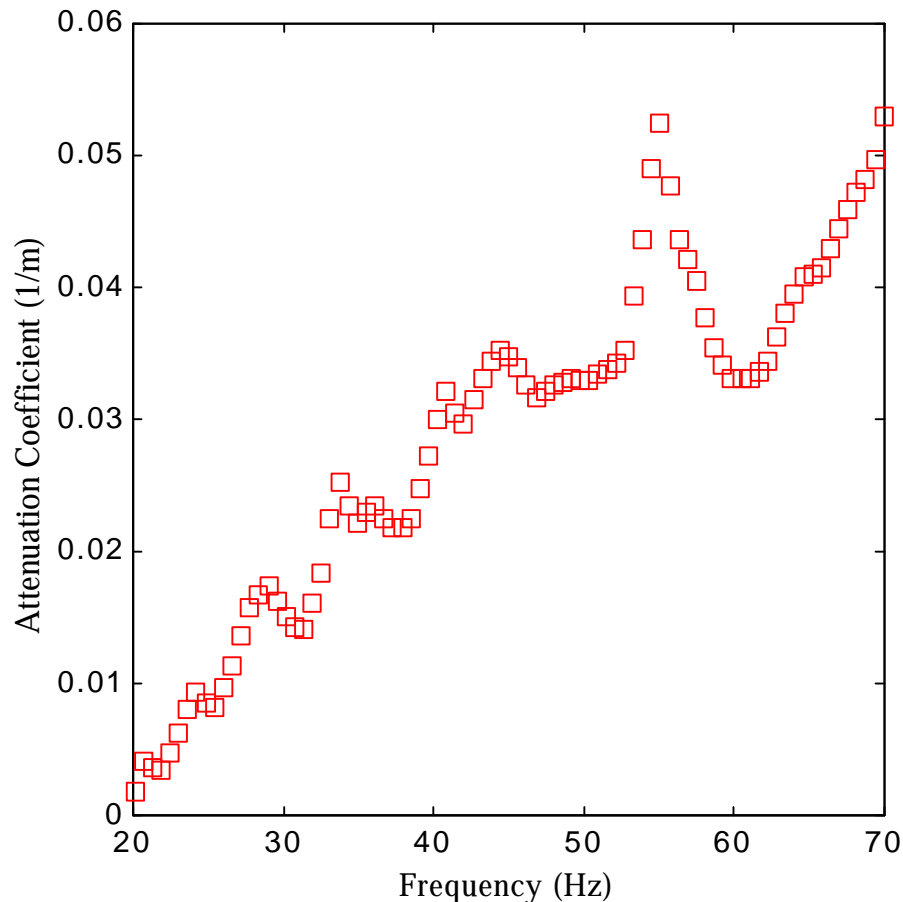


Figure 7.8 ISC '98 Attenuation Curve Estimate from Least Squares Fitting the Geometric Spreading Normalized Displacements

multiple modes. The large deviation near 55 Hz corresponds to the resonance effect observed in Chapter 6. The attenuation estimate from this method suffers several limitations. First, the estimate does not filter competing signals or remove ambient seismic energy. Some natural orthogonality reduces the effects of competing signals arriving from off-axis directions, since their wavelengths differ from the wavelength along the axis of the array. Second, the method does not explicitly account for multiple modes. The orthogonality between the longest and shorter wavelength modes relies on a large enough spatial distance to allow the orthogonality to develop. Since the spatial window and number of samples is limited, multiple modes and the sensor locations affect the attenuation estimate. Due to noise inclusion and incomplete filtering of competing signals, the attenuation coefficient estimated from a limited number of samples may not correspond to the minimum wavenumber.

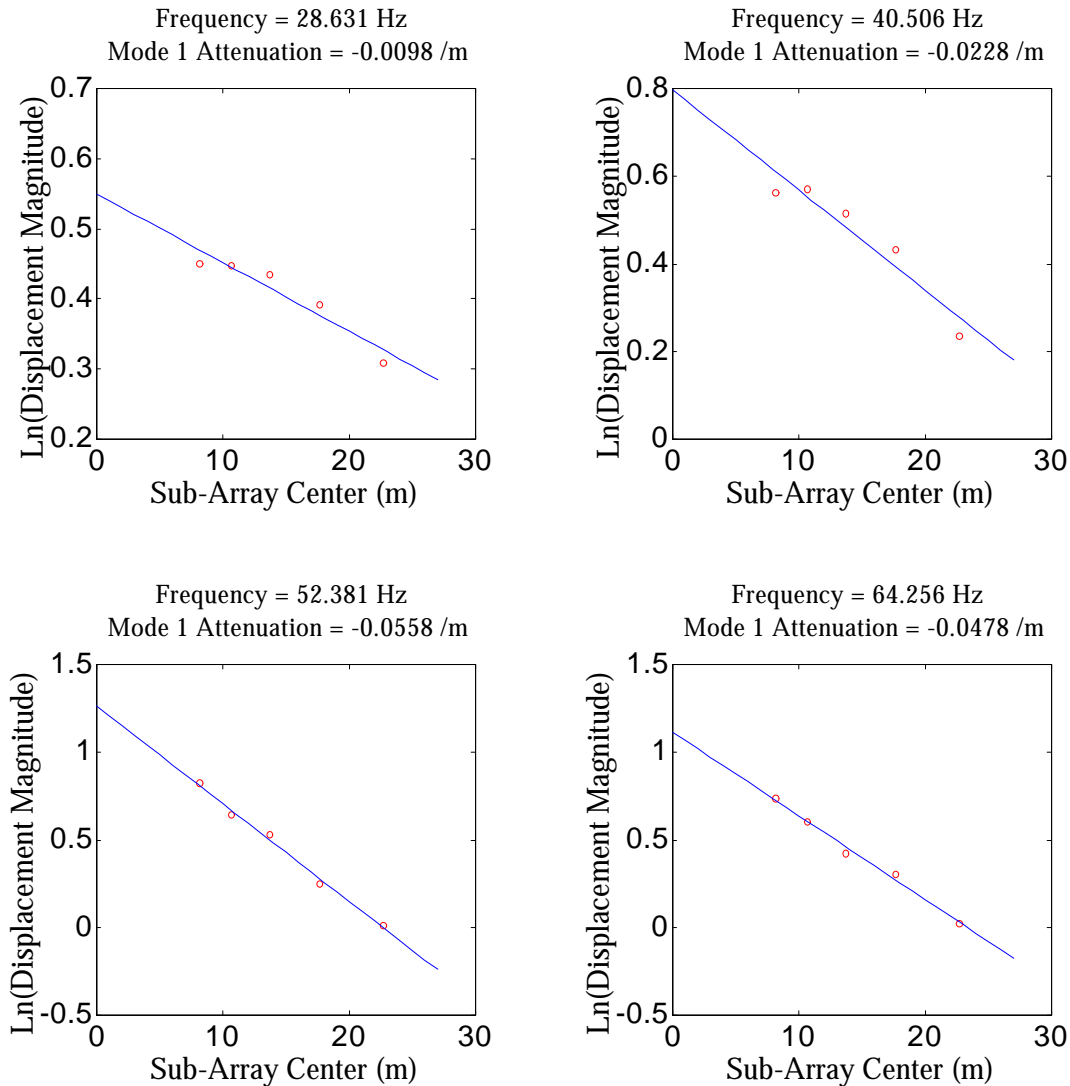


Figure 7.9 Dominant Mode Attenuation Coefficient Estimates Using 9 Sensor Sub-Arrays

7.6.3 Sub-Array Estimation of Dominant Mode Attenuation

The use of sub-arrays allows a decrease in the impacts due to competing signals. See Johnson and Dudgeon (1993) for an introduction of the use of sub-arrays in spectrum estimation. The use of sub-arrays creates a filter to attempt to block out competing signals, but does not reduce the ambient noise power in the estimate. A method to remove stationary noise will be presented in Section 7.6.5.

The dominant mode, sub-array attenuation coefficient estimates for several frequencies are shown in Figure 7.9. Nine sensor sub-arrays were used for the estimates. The sub-array amplitude estimates fit a linear trend, especially at the higher frequencies. The lower frequency estimates have a more sinusoidal nature due to a weaker orthogonality for the longer wavelengths at those frequencies. Figure 7.10 shows the dominant energy mode attenuation curve estimated with the sub-array method. The break to a different mode at about 45 Hz matches the trend seen in the dispersion curve estimates of the previous chapter.

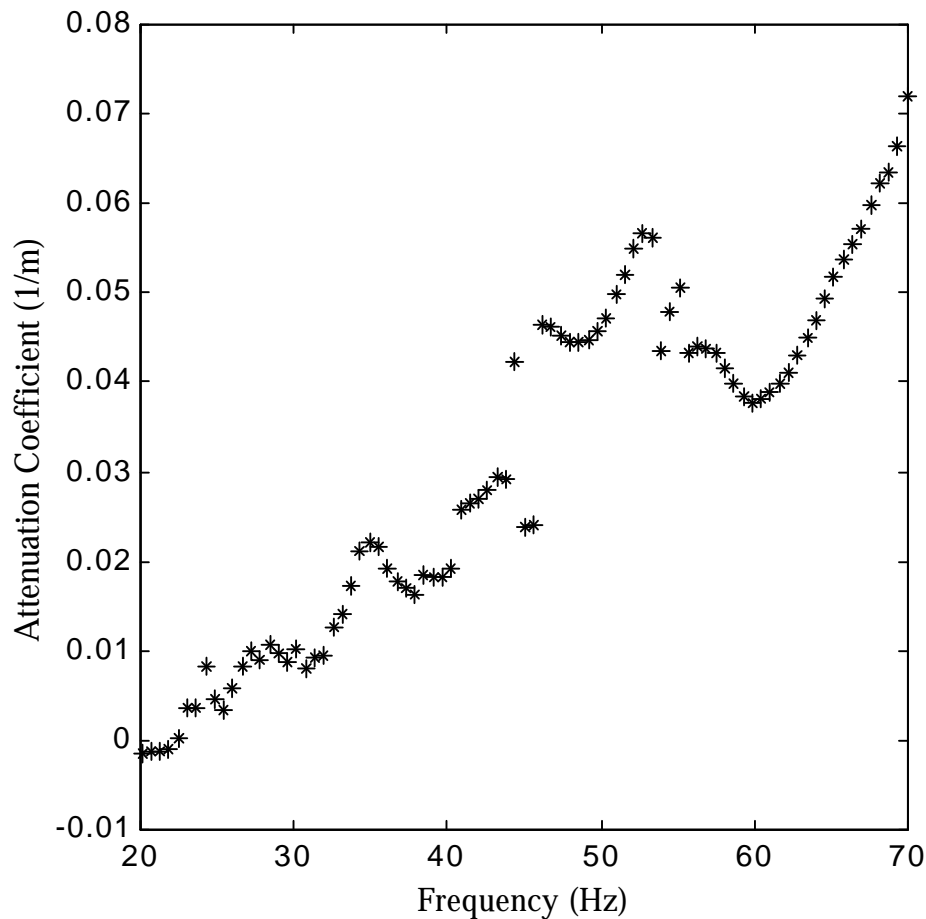


Figure 7.10 Dominant Mode Attenuation Curve Obtained from Sub-Array Estimation Method

7.6.4 Sub-Array Estimation of Multimodal Attenuation Coefficients

Due to the ability of sub-arrays to estimate power contained in individual wavenumbers, multiple mode attenuation coefficients can be estimated. Figure 7.11 shows the attenuation coefficient estimate for the mode with the second greatest energy content at several frequencies. The least square fits are excellent, but the sinusoidal nature of the deviations due to incomplete orthogonality are seen in the estimates. Figure 7.12 shows the multimodal attenuation curve for the ISC '98 site. The estimates for the two modes tend to converge at high frequencies, which is expected due to decreasing wavelengths. Figure 7.13 shows attenuation versus wavelength.

Surface waves with equal wavelengths may penetrate the soil to different depths, e.g. due to waveguide effects, and therefore the same wavelength surface wave may have

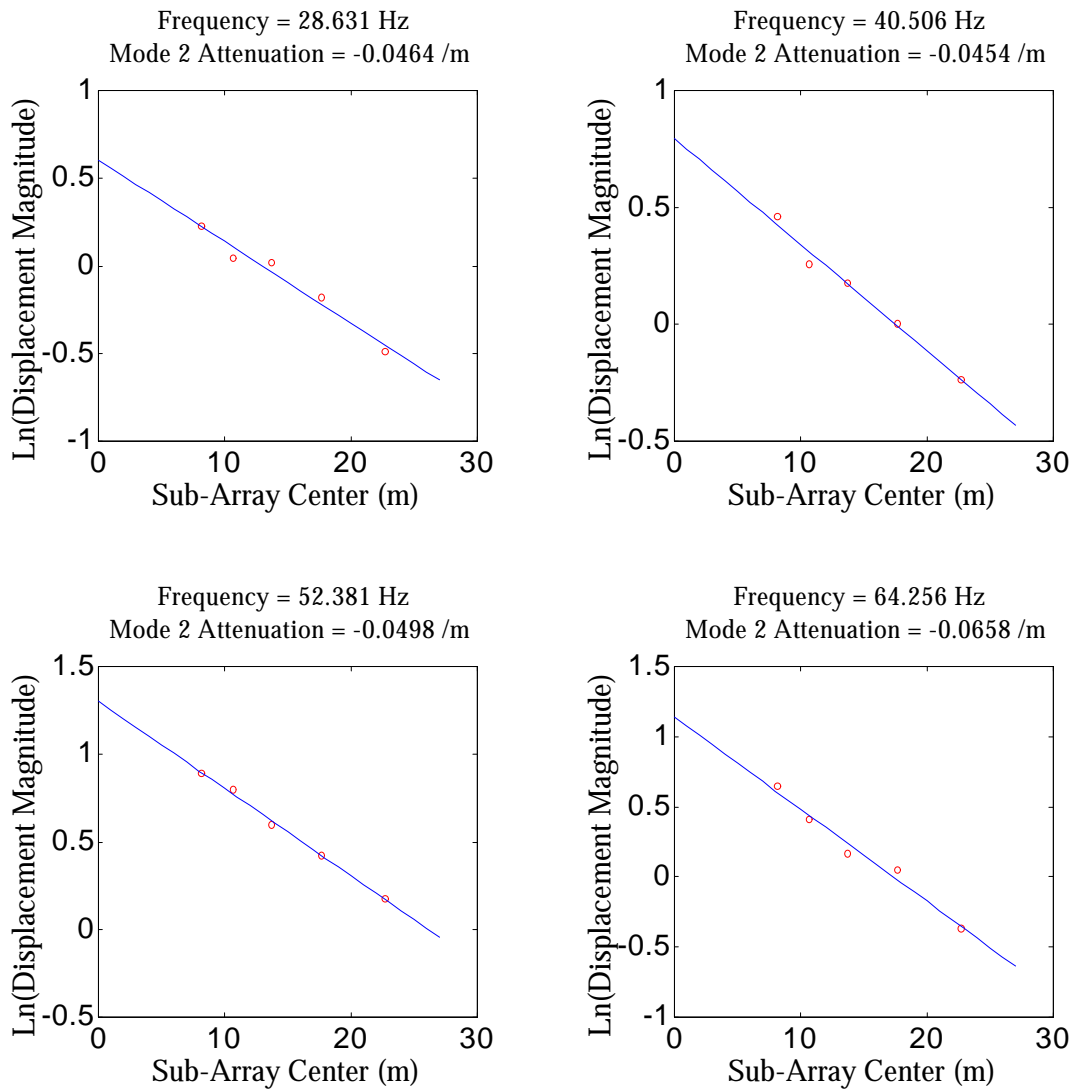


Figure 7.11 Multiple Mode Attenuation Coefficient Estimate. The attenuation coefficient is estimated for the wavenumber modes with the second greatest energy content.

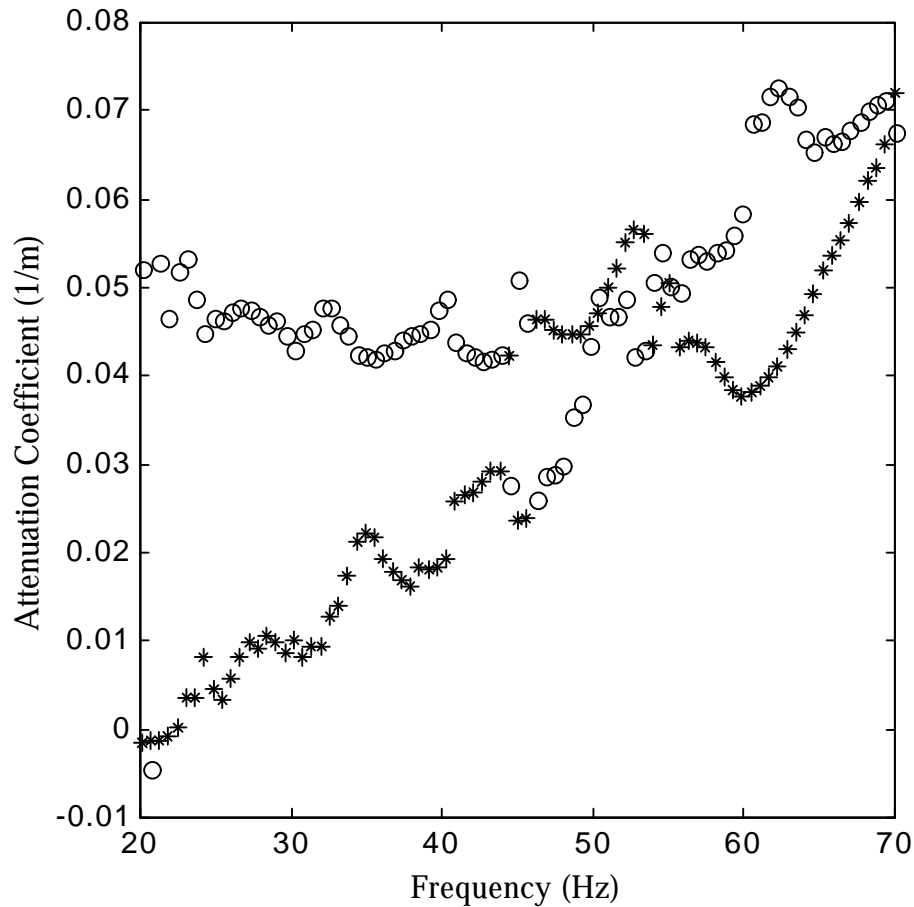


Figure 7.12 Multiple Mode Attenuation Curves for ISC '98 Site: Attenuation Versus Frequency. The dominant energy mode (asterisks) and the mode with the second greatest energy content (circles) are shown.

different material attenuation coefficients. The almost flat curve estimated for the second mode is tenable if viewed in terms of waveguides. If the second mode is due to the reflection of different frequency waves at the same interface or curved ray paths in gradually varying media, and the waves propagate within the same layer or layers, the attenuation will be approximately equal. Additionally, the wavelengths will vary due to the difference in the phase of reflected energy at different wavelengths.

7.6.5 Stationary Noise Removal

Stationary noise power can be removed with two procedures. First, the minimum power estimated from the power spectrum estimate, i.e. in a region remote from a signal peak, can be subtracted from the sub-array power estimates. Second, eigenanalysis provides a more pleasing alternative, since the noise power in the exact spatio-spectral correlation matrix estimates equals the minimum eigenvalue (Johnson and Dudgeon, 1993). This relationship stems directly from the eigenvalue extremal property of power spectrum

estimation (Hayes, 1996). Noise removal affects the ISC '98 attenuation coefficient estimates minimally, probably due to the large power output of the active source relative to the ambient seismic background.

7.7 Far-Field, $x^{-0.5}$ and Cylindrical Model Comparison

The far-field, \sqrt{x} decay rate forces cylindrically spreading Rayleigh surface waves to fit the incorrect physical model. The effects on the estimated Rayleigh wave amplitude and material attenuation are different, depending on the assumptions about the model parameters. This section will discuss the effects of the model incompatibility on traditional attenuation estimates and compare the traditional estimates with the cylindrical model estimates.

7.7.1 Far-Field Approximation when Signal Amplitude Unknown

If the regression procedure chooses the intercept, minimization of the squared error between the \sqrt{x} model and experimental measurements can focus on the points further

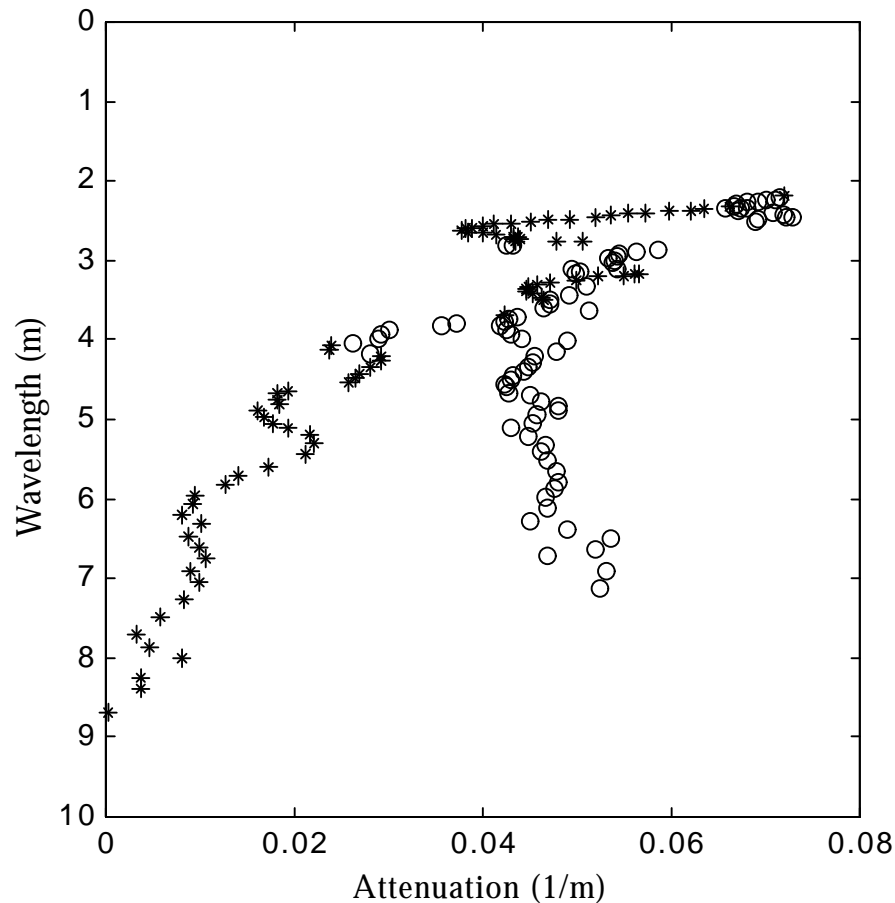


Figure 7.13 Multiple Mode Attenuation Curves for ISC '98 Site: Attenuation Versus Wavelength. The dominant energy mode (asterisks) and the mode with the second greatest energy content (circles) are shown.

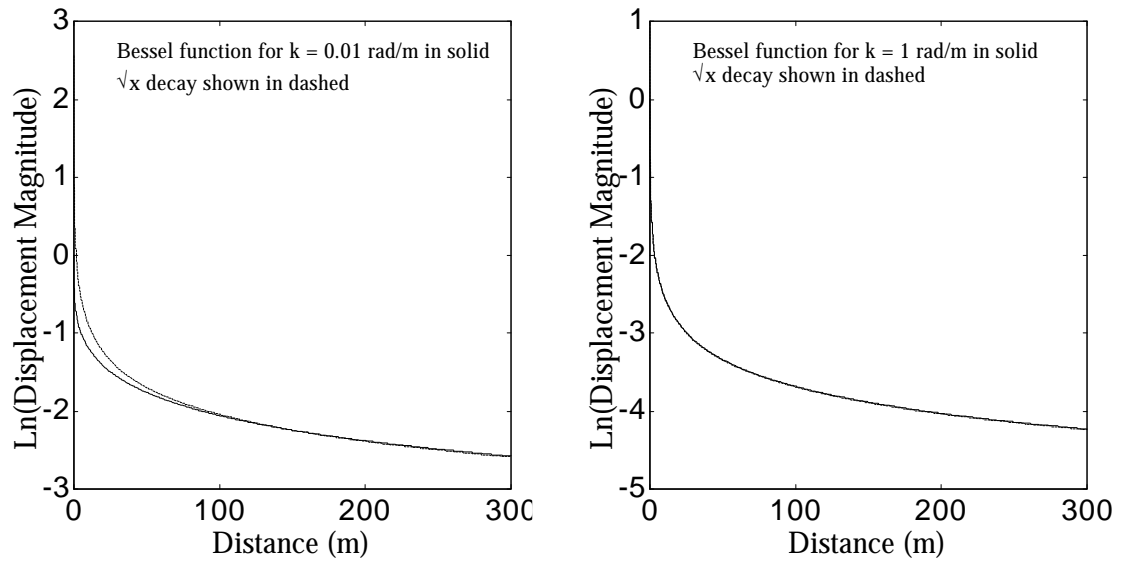


Figure 7.14 Model Incompatibility I: Free Intercept. The cylindrical Bessel function solution (solid line) is shown for wavenumbers equal to 0.01 rad/m (left panel) and 1 rad/m (right panel). The \sqrt{x} model (dashed line) is shown with free intercept to maximize model convergence to the cylindrical model in the far-field. In both panels the intercept for the Bessel functions are 0, on a natural logarithm scale, while the \sqrt{x} model intercepts are 2.56 (left panel) and 0.91 (right panel).

from the source. Figure 7.14 shows the difference between the correct cylindrical wavefield model intercept and the \sqrt{x} model for two example wavenumbers. The \sqrt{x} model does not yield the correct intercept in either case, but the \sqrt{x} model looks more applicable for the larger wavenumber.

7.7.2 Far-Field Approximation when Signal Amplitude Assumed Known

If the wave amplitude is assumed known, the model incompatibility effects have a different impact on the material attenuation estimate. Figure 7.15 shows two cylindrical wavefields and the \sqrt{x} model using the correct amplitude. The \sqrt{x} model fits neither wavefield very well, and the misfit displays the difference in geometric spreading between the cylindrical wave equation Bessel solutions and the \sqrt{x} model. As an additional comment, if the amplitude of the surface wave is fixed incorrectly, e.g. if the source magnitude is used as the intercept even though only a portion of the energy contributes to Rayleigh waves, then the error in the attenuation estimate will be larger and less conservative.

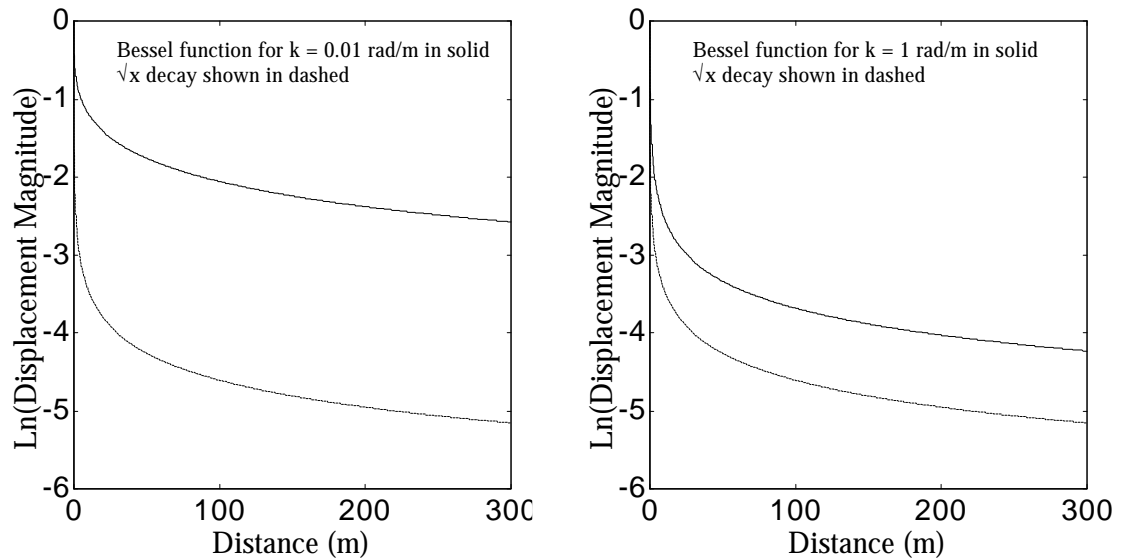


Figure 7.15 Model Incompatibility II: Known Intercept. The cylindrical Bessel function solution (solid line) is shown for wavenumbers equal to 0.01 rad/m (left panel) and 1 rad/m (right panel). The \sqrt{x} model (dashed line) is shown with intercept fixed to the correct cylindrical amplitude, which is 0. Notice the large deviation of the \sqrt{x} from the cylindrical models.

7.7.3 Model Incompatibility Effects on Attenuation Estimates

The effects, when allowing the regression to choose the intercept, include the following:

- 1.) The material attenuation estimates are biased, but asymptotically unbiased as frequency increases,
- 2.) The material attenuation estimates are unconservative, since the material attenuation must compensate for using too small a geometric spreading rate.

7.8 Discussion

Figure 7.16 compares the minimum wavenumber and dominant mode attenuation coefficients. In a profile with increasing damping with depth, the minimum wavenumber attenuation estimate should be lower for all frequencies, but due to noise inclusion, the samples are greater for some frequencies. At larger frequencies, and shorter wavelengths, the minimum wavenumber material attenuation estimates do yield a lower attenuation estimate because of a larger spatial distance relative to wavelength for the orthogonality properties to develop. The general trends of the minimum wavenumber and dominant mode attenuation estimates are the same, but the sub-array dominant mode estimator appears to isolate an additional mode from about 45 to 55 Hz.

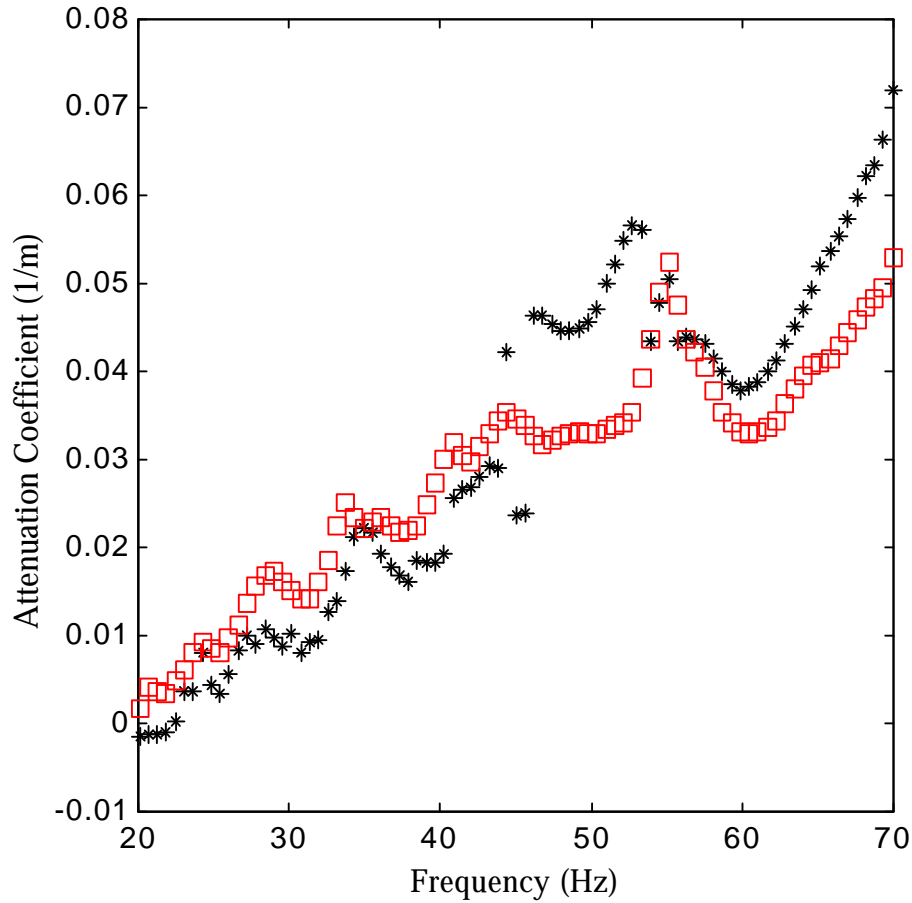


Figure 7.16 Comparison of Minimum Wavenumber (squares) and Sub-Array Dominant Mode (asterisks) Attenuation Estimates

As discussed in the previous section, the \sqrt{x} model would be expected to yield unconservative attenuation estimates. The \sqrt{x} model resembles the minimum wavenumber attenuation estimate, since all the magnitude estimates are combined without attempting to filter competing waves. Figure 7.17 compares the \sqrt{x} model attenuation estimates, obtained by allowing the regression to determine the intercept, and the minimum wavenumber attenuation estimate. The trends are almost identical, with the \sqrt{x} model estimates always plotting above the minimum wavenumber estimates. The convergence of the two estimates as frequency increases supports the asymptotically unbiased nature of the \sqrt{x} model attenuation estimates.

At lower frequencies, below about 20 Hz, the minimum wavenumber and sub-array dominant mode estimators yield attenuation estimates that imply an increase in energy with distance, i.e. attenuation estimates with the incorrect sign. The estimation of a physically impossible quantity is explained by the resolution of the array. Figure 7.18 shows the attenuation estimates for relatively low frequencies. The cutoff for the correct sign on the attenuation estimates corresponds to the point at which single wavenumbers can be isolated, i.e. the frequency-wavelength pair at which the array can resolve a single wavenumber. If single wavenumbers cannot be isolated, an incorrect geometric spreading function is used to normalize the wavefield. As shown in Figure 7.17, the far-field \sqrt{x} attenuation estimates never become negative. Although a more pleasing physical result, the nonnegative estimates stem from a compensation for using a too low geometric spreading loss.

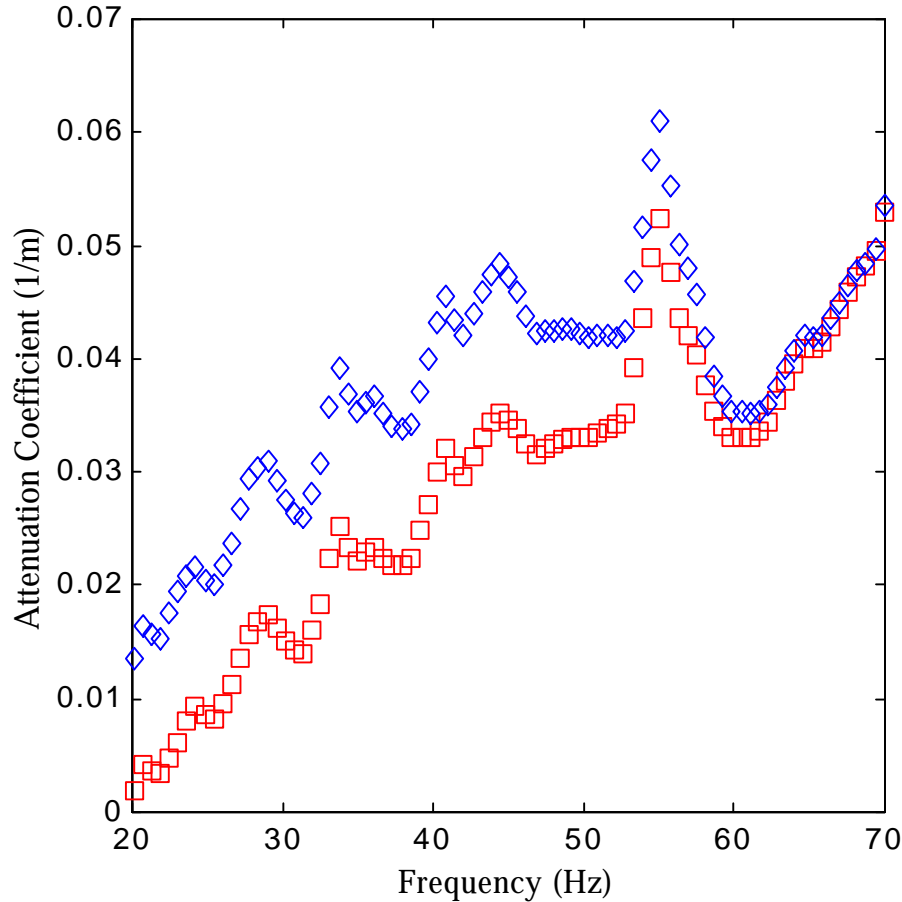


Figure 7.17 Comparison of \sqrt{x} Model (diamonds) and Minimum Wavenumber (squares) Attenuation Estimates

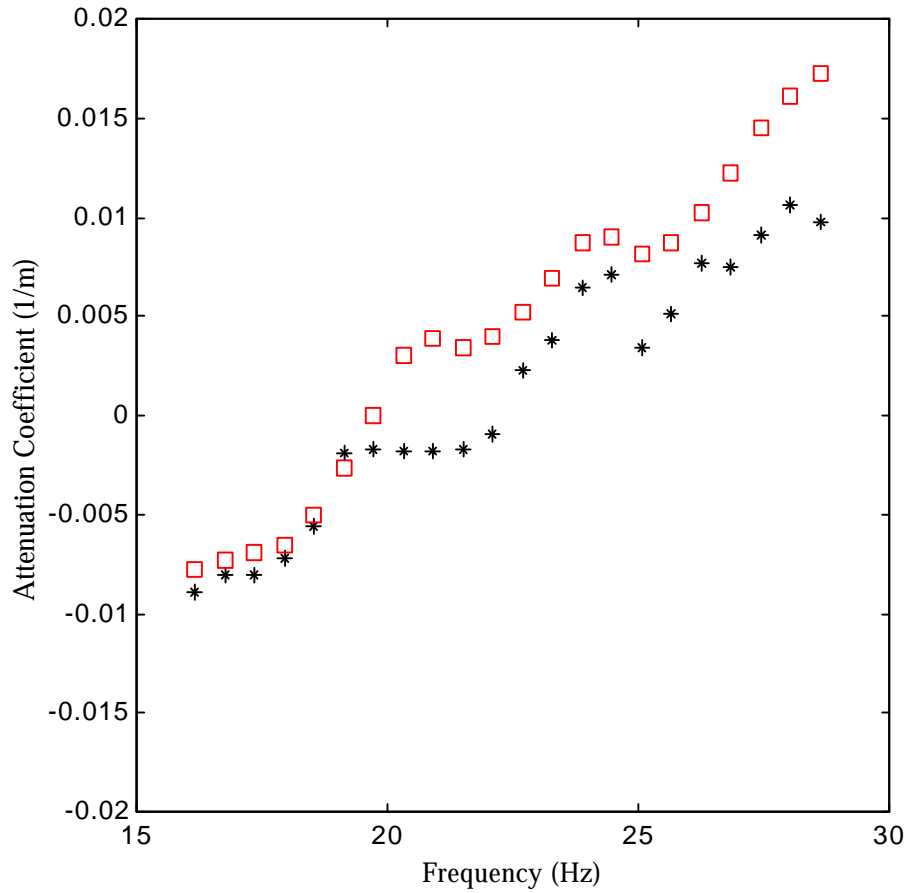


Figure 7.18 Limited Resolution Effects on Attenuation Estimation. The minimum wavenumber (squares) and sub-array dominant mode (asterisks) attenuation estimates are shown.

7.9 Summary and Conclusions

The \sqrt{x} model represents only an approximation to the correct physics of cylindrical spreading Rayleigh surface waves. The use of the Bessel function solution to the cylindrical wave equation and optimum wavenumber estimates allows geometric spreading to be removed. Different cylindrical wavenumbers decay at different rates, which explains the previous observations of site-dependent geometric spreading functions (Lai, 1998). The geometric spreading and cylindrical propagation model for Rayleigh surface waves was discussed, and the correct model was used to obtain dominant and multimodal attenuation coefficients.